Journal of Sound and Vibration (1997) **207**(5), 601–616

INFLUENCE OF CROSS-SECTIONAL SHAPE ON THE CONDUCTIVITY OF A WALL APERTURE IN MEAN FLOW

M. S. Howe

Boston University, *College of Engineering*, 110 *Cummington Street*, *Boston*, *MA* 02215, *U.S.A*

(*Received* 18 *December* 1996, *and in final form* 25 *April* 1997)

An analysis is made of the effect of cross-sectional shape on the motion induced in a wall aperture by a pressure perturbation in the presence of high Reynolds number tangential flow. Previous studies for circular and rectangular apertures indicate that there is a transfer of energy from the applied perturbation to the mean flow (via the production of vorticity in the aperture) provided the Strouhal number based on aperture diameter and mean velocity is small. In this paper apertures are considered whose cross-sections are symmetrically tapered in a direction parallel to the mean flow. For highly tapered apertures of trapezoidal cross-section, it is found that low Strouhal number damping is confined to a smaller range of frequencies. Self-sustaining oscillations of the shear layers spanning the aperture can occur at certain discrete frequencies, which correspond to the real parts of complex eigenfrequencies of the aperture motion having *positive* imaginary parts. The eigenfrequencies are poles of the Rayleigh conductivity, and are found to vary in proportion to U/L, where U is mean flow speed and L is the maximum streamwise length of the aperture, but to be only weakly dependent on aperture shape.

1. INTRODUCTION

Sound incident on small apertures in the presence of mean flow is frequently dissipated via the production of vortical kinetic energy that is swept away by the flow [1]. The absorption can be enhanced over well defined ranges of frequencies when the apertures are backed by resonant cavities [2, 3]. Under certain conditions, narrow band acoustic tones may be generated spontaneously at the aperture, even when the mean flow is nominally steady and there is no applied pressure [4]. The tones are often heard over distinct "operating stages" within which the Strouhal number based on aperture dimension and mean flow velocity varies over a finite range controlled by an acoustic or hydrodynamic *feedback*. The feedback is related to the periodic shedding of vorticity from an edge, its convection over the aperture, and the subsequent production of impulsive pressures when the vorticity impinges on a downstream edge [5]. The tonal amplitude varies with flow speed and exhibits discontinuous changes in frequency as the system jumps between different operating stages, in accordance with various well known empirical laws [5–9].

0022–460X/97/450601 + 16 $25.00/0/sv971103

There is no general theory of feedback controlled by vortex shedding at arbitrary Mach numbers (particular approximations are discussed in references [10–15]), but a deductive theory of the resonance stages has been proposed by the author [16] for cases of low Mach number, high Reynolds number flow over an acoustically compact aperture in a plane wall. The Strouhal number of an operating stage is identified with the real part of a pole in the upper half of the complex frequency plane of the Rayleigh conductivity of the aperature [17]. The conductivity is calculated according to linear perturbation theory, by approximating the shear layer over the aperture by a *linearly* disturbed vortex sheet. Non-linearity must limit the growth of instabilities predicted by this approach, but it is argued that the finite amplitude of the real motion will not significantly change Strouhal number predictions of linear theory, because feedback is controlled by the convection velocity U_c of disturbances across the aperture, which experiments suggest to be effectively independent of amplitude [18–20]. Further justification is given in reference [16], where predictions (based on the same theory) of the operating stages of jet-edge interactions and shallow wall cavities are shown to be in excellent agreement with experiment.

The theory of reference [16] is applicable to rectangular apertures in a wall of infinitesimal thickness, and is an extension of a numerical investigation of the conductivity of a circular aperture in the presence of flow performed by Scott [21, 22]. The influence of small, but finite wall thickness is considered in reference [23]. In applying idealized models of this kind to practical problems involving, say, the interaction of sound waves with a sparsely perforated screen in a mean flow, it is also desirable to know the likely effects of varying the shape of the aperture cross-section (for shapes other than circular or rectangular). It would then be possible to ascertain, for example, whether it is possible to optimize the attenuation of sound by the screen by a suitable adjustment of aperture shape and dimensions. Similar considerations are important for vortex shedding devices used to absorb structural vibrations [24].

In this paper the influence of cross-sectional shape for a class of ''tapering'' apertures that have one straight edge normal to the flow, and an axis of symmetry parallel to the mean flow direction is investigated. Predictions are given for cases involving flow on one or both sides of the wall at very high Reynolds number, when free shear layers may be modelled by vortex sheets. The motion is stable when the mean flow is the same on both sides of the wall and the wall has negligible thickness (when, for an ideal fluid, the mean vorticity vanishes in the steady state [22]), but becomes unstable at finite thickness, giving rise to self-sustaining aperture oscillations and sound generation. One-sided flow over the aperture (which is then spanned by a plane vortex sheet in the undisturbed state) is always unstable, and finite wall thickness merely changes the Strouhal numbers of the self-sustained oscillations. Reverse flow reciprocity can be invoked to argue that the conductivity and instability Strouhal numbers are unchanged when the direction of the mean flow is reversed. Detailed results are presented for an aperture of trapezoidal cross-section that is symmetric with respect to the direction of the mean flow. It is concluded that permissible Strouhal numbers of self-sustained oscillations for symmetric shapes of this kind scale with the maximum aperture dimension in the streamwise direction, but that the damping of an incident pressure field at low Strouhal numbers is confined to progressively smaller frequencies as the tapering increases.

The analytical model is formulated in section 2 for a general symmetric, tapering aperture in the presence of an arbitrary, two-sided, low Mach number, high Reynolds number flow. Specific results are given in sections 3, 4 respectively for two-sided uniform flow and one sided flow past an aperture of trapezoidal cross-section.

2. THE GOVERNING EQUATIONS

2.1. THE RAYLEIGH CONDUCTIVITY

Consider fluid of uniform mean density ρ_0 in nominally steady, low Mach number, high Reynolds number flow over both sides of an aperture in a plane, rigid wall of thickness d. The midplane of the wall coincides with the plane $x_2 = 0$ of the rectangular co-ordinate system (x_1, x_2, x_3). The mean flow is parallel to the x_1-axis with main stream velocities U_+ and U_- in the "upper" and "lower" regions $x_2 \gtrless \pm 1/2d$ respectively. Attention is confined to the set of tapering apertures of the type illustrated schematically in Figure 1. The "leading edge" of the aperture is assumed to be straight, and to occupy the interval $x_1 = -s \equiv -L/2$, $|x_3| < b_0/2$, where L denotes the maximum length of the aperture in the streamwise direction, and b_0 is the maximum spanwise dimension (at the leading edge). Over the interval $-s < x_1 < s$ of length L, the aperture is symmetric about the x_1-axis, with side edges defined in the x_1x_3-plane by $x_3 = \pm b(x_1)/2$, where $b(x_1)$ is required to be either constant or to decrease monotonically with x_1. The shear layers over the upper and lower faces of the aperture are modeled by vortex sheets, and the fluid within the volume of the aperture (in $|x_2| < 1/2d$) is taken to be in a mean state of rest.

Uniform, small amplitude, time-dependent pressures $p_\pm(t)$ are applied in the vicinity of the aperture respectively in the upper and lower regions. The resulting disturbances of the vortex sheets are assumed to be governed by linearized equations of motion. The aperture volume flux $Q(t)$ produced by the pressure differential

$$[p_0(t)] \equiv p_+(t) - p_-(t)$$

can be expressed in the form

$$\rho_0 \partial Q(t)/\partial t = -\int_{-\infty}^{\infty} K_R(\omega)\,[p_0(\omega)]e^{-i\omega t}\,d\omega, \tag{1}$$

where $K_R(\omega)$ is the Rayleigh conductivity [17], which is a function of the radian frequency ω with the dimensions of length, and $[p_0(\omega)] = (1/2\pi)\int_{-\infty}^{\infty}[p_0(t)]e^{i\omega t}\,dt$ is the Fourier transform of $[p_0(t)]$.

For time-harmonic fluctuations, where $[p_0(t)] \equiv \mathrm{Re}\{[p_0(\omega)]e^{-i\omega t}\}$, the power $\Pi(\omega)$

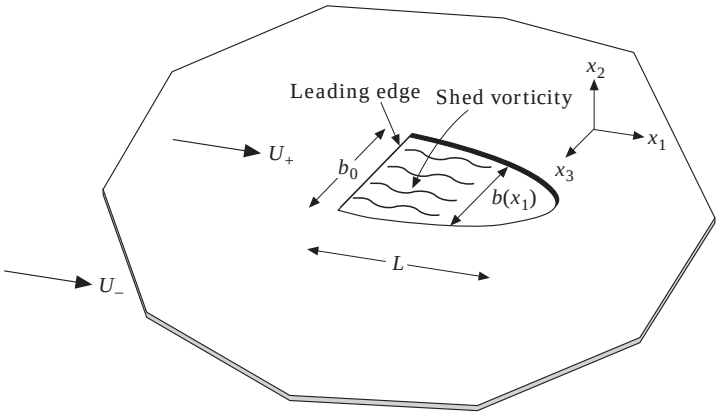

Figure 1. Two-sided flow over a symmetric, tapered aperture with a straight leading edge in a wall of thickness d.

dissipated at the aperture by the applied pressure field can be expressed in terms of the conductivity by making use of the formula

$$\Pi \equiv -\langle Q(t)\,[p_0(t)]\rangle,$$

where the angle brackets denote a time average. This yields (for $\omega > 0$)

$$\Pi(\omega) = -|[p_0]|^2 \mathrm{Im}\{K_R(\omega)\}/2\rho_0\omega. \tag{2}$$

Direct thermo-viscous losses are usually negligible at high Reynolds numbers, when most of the dissipation is caused by the transfer of energy from the applied pressure (an incident sound wave, say) to the kinetic energy of vorticity generated in the aperture. Equation (2) shows that this occurs provided $\mathrm{Im}\{K_R(\omega)\} < 0$ (when $\omega > 0$). The damping is *negative* if $\mathrm{Im}\{K_R(\omega)\} > 0$, in which case energy is *extracted* from the mean flow. When the fluid is compressible Q determines the amplitude of an effective acoustic monopole source at the aperture, and a net gain in perturbation energy would result in increased levels of radiation from the aperture on either side of the wall

In practice an arbitrary flow disturbance can trigger instabilities of the aperture flow, and result in oscillations and acoustic radiation at one or more preferred frequencies. These instabilities are associated with singularities of the conductivity $K_R(\omega)$ in the upper half of the complex frequency plane [16]. Indeed, although equation (1) determines $Q(t)$ in terms of the applied pressure differential $[p_0(t)]$, a strictly *casual* evaluation of the integral requires the path of integration from $\omega = \pm\infty$ to pass *above* the singularities of the integrand in the ω-plane. Since $p_\pm(t)$ may be assumed to vanish prior to some finite time in the past, $[\mathrm{p}_0(\omega)]$ is regular in $\mathrm{Im}\{\omega\} > 0$, and any singularities are associated with the conductivity $K_R(\omega)$. These singularities are simple poles for circular and rectangular apertures [16, 21–23], and will be shown to be poles also for the set of apertures discussed in this paper. Experiments on jet-edge interactions and shallow wall cavities, for which the same type of theory is applicable, indicate [16] that the real part of the complex frequency at these poles, determined according to idealized, linear perturbation theory, may be identified with the frequency of an operating stage of the self-sustained oscillations of the aperture flow for the real, non-linear system.

2.2. THE THIN WALL APPROXIMATION

The equations of motion of the vortex sheets spanning the aperture openings of Figure 1 are similar to those discussed in references [16, 22] for circular and rectangular apertures in a wall of zero thickness, and only a brief outline of the derivation is needed here.

Let the aperture be excited by a time-harmonic, uniform pressure differential $[p_0(\omega)]\mathrm{e}^{-\mathrm{i}\omega t}$, and denote respectively by $\zeta_\pm(x_1, x_3)\,\mathrm{e}^{-\mathrm{i}\omega t}$ the displacement (in the x_2 direction) of the upper and lower vortex sheets from their undisturbed positions $x_2 = \pm 1/2d$. The flow Mach numbers are assumed to be sufficiently small that the motion in the neighborhood of the aperture may be treated as incompressible, so that the following linearized formulae for the perturbation pressures above and below the wall are applicable:

$$p = p_+ - \rho_0\left(\omega + \mathrm{i}U_+\frac{\partial}{\partial x_1}\right)^2 \int_s \frac{\zeta_+(y_1, y_3)}{2\pi|\mathbf{x}-\mathbf{y}|}\,\mathrm{d}y_1\,\mathrm{d}y_3, \qquad x_2 > \tfrac{1}{2}\mathrm{d},$$

$$= p_- + \rho_0\left(\omega + \mathrm{i}U_-\frac{\partial}{\partial x_1}\right)^2 \int_s \frac{\zeta_-(y_1, y_3)}{2\pi|\mathbf{x}-\mathbf{y}|}\,\mathrm{d}y_1\,\mathrm{d}y_3, \qquad x_2 < -\tfrac{1}{2}\mathrm{d}, \tag{3}$$

where respectively $\mathbf{y} = (y_1, \pm 1/2d, y_3)$, the integration is over the aperture cross-section S, and the exponential time factor $e^{-i\omega t}$ is here and henceforth suppressed.

The *thin wall* approximation is now introduced, in which the wavelength of vortex sheet motions is restricted to be large compared to the wall thickness d. The x_2-component ζ of the fluid displacement within the aperture may then be regarded as independent of x_2, i.e.,

$$\zeta \equiv \zeta(x_1, x_3) = \zeta_+(x_1, x_3) = \zeta_-(x_1, x_3), \tag{4}$$

and the equation of motion of a "column" of fluid within the aperture is

$$\rho_0 d\partial^2\zeta/\partial t^2 = -[p], \qquad |x_1| < s, \qquad |x_3| < \tfrac{1}{2}b(x_1), \tag{5}$$

where $[p]$ is the difference in the pressures applied to the upper and lower ends of the column at $x_2 = \pm 1/2d$, determined by equations (3). Thus, substituting from equation (3) into equation (5) one finds, for time-harmonic motion,

$$\left[\left(\omega + iU_+\frac{\partial}{\partial x_1}\right)^2 + \left(\omega + iU_-\frac{\partial}{\partial x_1}\right)^2\right]\frac{1}{2\pi}\int_s \frac{\zeta(y_1, y_3)\,dy_1\,dy_3}{\sqrt{(x_1 - y_1)^2 + (x_3 - y_3)^2}} + d\omega^2\zeta(x_1, x_3) = \frac{[p_0]}{\rho_0}. \tag{6}$$

According to Figure 1 the aperture motion involves the unsteady shedding of vorticity from the straight leading edge $x_1 = -s$ of the aperture. Equation (6) is considerably simplified by means of the hypothesis that this shedding produces strongly correlated motions of the vortex sheets at different transverse locations x_3, and that ζ may therefore be assumed to be independent of x_3. To be sure, observations [11–13,15] suggest that, although the laterally uniform shed vorticity interacts with different parts of the downstream edge at different times, the aggregate back reaction on the leading edge is equivalent to an average back reaction that causes the stability characteristics to be the same as those of a rectangular aperture of intermediate length. By explicitly performing the integration in equation (6) with respect to y_3 over the interval $-1/2b(y_1) < y_3 < 1/2b(y_1)$, and also integrating the equation with respect to x_3 (over $-1/2b(x_1) < x_3 < 1/2b(x_1)$), one can then re-cast equation (6) in the dimensionless form

$$\left[\left(\sigma + i\frac{\partial}{\partial\xi}\right)^2 + \left(\sigma + i\mu\frac{\partial}{\partial\xi}\right)^2\right]\int_{-1}^{1} Z(\eta)\{1n|\xi - \eta| + \mathscr{L}(\xi, \eta)\}\,d\eta - \pi\left(\frac{d}{s}\right)\sigma^2 Z(\xi) = 2\sigma^2\bar{\beta}(\xi), \qquad |\xi| < 1, \tag{7}$$

where Z is an effective dimensionless displacement defined by

$$Z(\xi) = (-2\rho_0\omega^2 s/\pi[p_0]b_0)b(\xi)\zeta(\xi), \tag{8}$$

and

$$\sigma = \omega s/U_+, \qquad \mu = U_-/U_+, \qquad \xi = x_1/s, \qquad \eta = y_1/s, \tag{9}$$

$$\begin{aligned}\mathscr{L}(\xi, \eta) = [1/2\beta(\eta)]\,([\beta(\xi) - \beta(\eta)]1n\,[\beta(\xi) - \beta(\eta) + \sqrt{(\xi - \eta)^2 + \{\beta(\xi) - \beta(\eta)\}^2}] \\ -[\beta(\xi) + \beta(\eta)]1n\,[\beta(\xi) + \beta(\eta) + \sqrt{(\xi - \eta)^2 + \{\beta(\xi) + \beta(\eta)\}^2}] \\ -\sqrt{(\xi - \eta)^2 + \{\beta(\xi) - \beta(\eta)\}^2} + \sqrt{(\xi - \eta)^2 + \{\beta(\xi) + \beta(\eta)\}^2}])\end{aligned} \tag{10}$$

$$\beta(\xi) = b(x_1)/2s, \qquad \bar{\beta}(\xi) = b(x_1)/b_0 \equiv (2s/b_0)\beta(\xi). \tag{11}$$

One next integrates equation (7) with respect to the second order differential operator on the left side by introducing the Green's function

$$G(\xi, \eta) = [1/2\sigma(1-\mu)]\,(H(\xi-\eta)\,e^{i\sigma_+(\xi-\eta)} + H(\eta-\xi)\,e^{i\sigma_-(\xi-\eta)}), \tag{12}$$

which is a particular solution of

$$[(\sigma + i\,\partial/\partial\xi)^2 + (\sigma + i\mu\,\partial/\partial\xi)^2]G(\xi, \eta) = \delta(\xi-\eta).$$

In these formulae, $H(x)$ is the Heaviside unit function ($=0, 1$ according to whether $x \lessgtr 0$), and $\sigma_\pm$ are the Kelvin–Helmholtz wavenumbers [25]

$$\sigma_\pm = \sigma((1 \pm i)/(1 \pm i\mu)). \tag{13}$$

By this means the effective displacement Z is found to satisfy

$$\int_{-1}^{1} Z(\eta)\{1n|\xi-\eta| + \mathscr{L}(\xi, \eta)\}\,d\eta - \pi\sigma^2(d/s)\int_{-1}^{1} Z(\eta)G(\xi, \eta)\,d\eta$$
$$+ \lambda_+ e^{i\sigma_+\xi} + \lambda_- e^{i\sigma_-\xi} = F(\sigma, \xi), \qquad |\xi| < 1, \tag{14}$$

where $\lambda_\pm$ are constants of integration, and $F(\sigma, \xi)$ is a particular integral of the term $2\sigma^2\overline{\beta}(\xi)$ on the right of equation (7) with respect to the second order differential operator.

The integral equation (14) is solved by collocation, by the procedure described by Scott [21] for a vortex sheet over a circular aperture. The values of $\lambda_\pm$ are fixed by imposing the Kutta condition that the vortex sheets should leave the upstream edge of the aperture smoothly, i.e., by requiring that $\zeta = \partial\zeta/\partial\xi = 0$ as $\xi \to -1$ [26], which is equivalent to

$$Z = \partial Z/\partial\xi = 0 \text{ at } \xi = -1. \tag{15}$$

Potential theory implies that the displacement has a mild, yet integrable singularity where the vortex sheet impinges on the downstream curvilinear aperture edge, at the worst proportional to the inverse square-root of the distance from that edge. This singularity is the linear theory representation of the large amplitude edge motion observed in practice.

The aperture volume flux is calculated from $Q(\omega) = -i\omega\int_{-s}^{s} b(x_1)\zeta(x_1)\,dx_1$, from which it follows that the Rayleigh conductivity is given in terms of Z by

$$K_R = -\frac{\pi}{2}\,b_0\int_{-1}^{1} Z(\eta)\,d\eta. \tag{16}$$

The conductivity is a complex valued function of the frequency ω, and also depends on the aperture shape, the wall thickness ratio d/L, and the mean velocity ratio $\mu = U_-/U_+$.

In the special case of uniform, two sided mean flow, where $U_- = U_+ \equiv U$, the wavenumbers σ_+ and σ_- are both equal to $\sigma = \omega s/U$, and Green's function (12) may be taken in the form

$$G(\xi, \eta) = -H(\xi-\eta)\,(\xi-\eta)\,e^{i\sigma(\xi-\eta)}. \tag{17}$$

The terms in $\lambda_\pm$ in equation (14) are now replaced by $(\lambda_1 + \lambda_2\xi)\,e^{i\sigma\xi}$, where λ_1, λ_2 are constants determined by the Kutta condition.

2.3. RECIPROCITY

A simple extension of the reverse flow reciprocal theorem [28, 29] can be used to show (see reference [22]) that the conductivity $K_R(\omega)$ determined by equation (16) for the aperture of Figure 1 is unchanged when the mean flow directions above and below the wall are reversed. The reciprocal theorem for an ideal fluid of uniform mean density implies that $\varphi(\mathbf{x}_B, \mathbf{x}_A, \omega) \equiv \varphi^R(\mathbf{x}_A, \mathbf{x}_B, \omega)$, where $\varphi(\mathbf{x}, \mathbf{x}_A, \omega)$, $\varphi^R(\mathbf{x}, \mathbf{x}_B, \omega)$ are the perturbation velocity potentials produced by equal volume point sources located respectively at $\mathbf{x}_A$ in the direct problem and at $\mathbf{x}_B$ in the reciprocal problem, provided the mean flow is reversed in the reciprocal problem. The theorem remains valid in the presence of vortex sheets spanning the wall aperture provided that, in both the direct and reciprocal problems, the sheets are *linearly* disturbed from their equilibrium positions, and the Kutta condition is satisfied at the appropriate "leading edge". In the reciprocal flow illustrated in Figure 2, the Kutta condition must be imposed at the curvilinear edge of the aperture, and this is precisely the case that defines the conductivity when the mean flow is reversed. The theorem has been confirmed by recent numerical studies [30] that do not invoke the lateral averaging approximation introduced above to simplify equation (6).

3. UNIFORM, TWO-SIDED FLOW OVER A TRAPEZOIDAL APERTURE

Equations (14) and (15) are now applied to the trapezoidal aperture depicted in planform in Figure 3(a). The aperture is symmetric with respect to the x_1-axis, with transverse ends at $x_1 = \pm s$ of lengths b_0 and b_1 ($\leqslant b_0$) respectively, in terms of which

$$\overline{\beta}(\xi) = 1 + \tfrac{1}{2}(b_1/b_0 - 1)\,\xi, \qquad F(\sigma, \xi) = \overline{\beta}(\xi) - \mathrm{i}(b_1/b_0 - 1)\,(1 + \mu)/\sigma. \tag{18}$$

In this section one considers the particular case in which the mean flows have equal speeds $U_+ = U_- \equiv U$ above and below the aperture.

3.1. DEPENDENCE OF RAYLEIGH CONDUCTIVITY ON b_1/b_0

In Figures 3(b) and 3(c) the real and imaginary components Γ_R, Δ_R of the dimensionless conductivity, defined by

$$K_R(\omega)/\sqrt{A} = \Gamma_R(\omega) - \mathrm{i}\Delta_R(\omega), \tag{19}$$

are plotted against real values of $\sigma = \omega s/U$, for $b_0/L = 1$ and $d = 0$, for the two characteristic cases $b_1/b_0 = 1$ and 0·1 respectively, where $A = s(b_0 + b_1) \equiv \frac{1}{2}L(b_0 + b_1)$ is

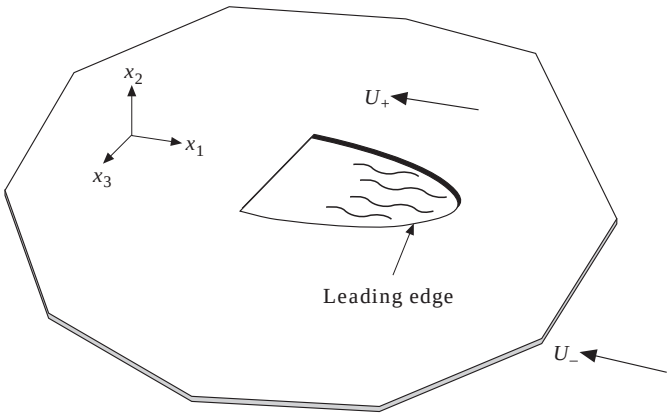

Figure 2. The reciprocal problem.

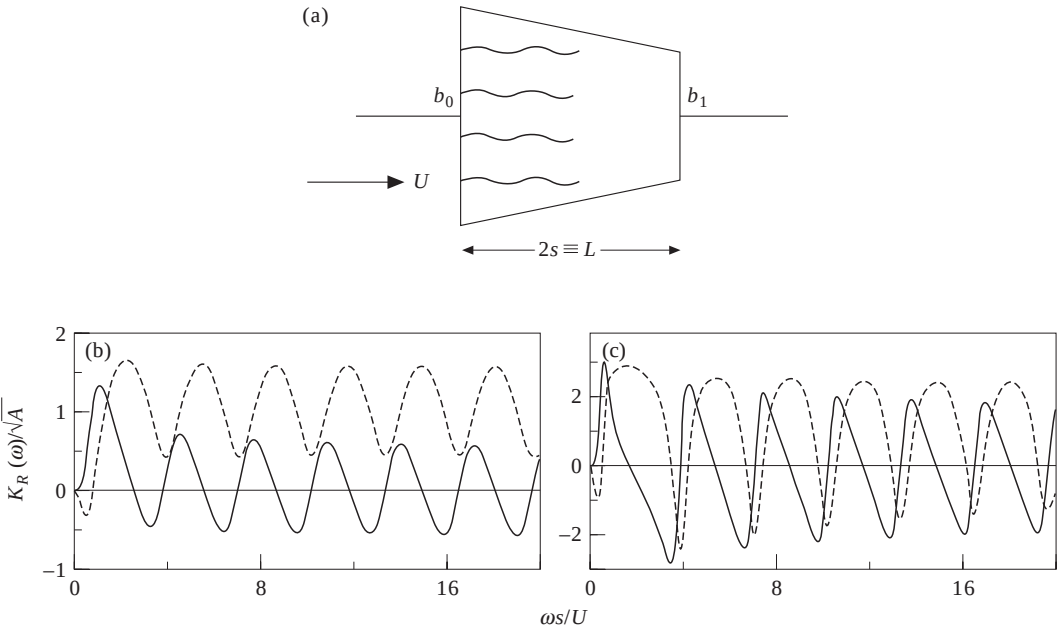

Figure 3. (a) Trapezoidal aperture; (b) the conductivity $K_R(\omega)/\sqrt{A} \equiv \Gamma_R(\omega) - i\Delta_R(\omega)$ for $U_- = U_+$ and $d/L = 0$ for a square aperture, $b_0/L = 1$, $b_1/b_0 = 1$; (c) conductivity for $b_0/L = 1$, $b_1/b_0 = 0{\cdot}1$; two sided uniform flow. Key: —, Δ_R; ---, Γ_R.

the area of the aperture. The first of these corresponds to a square aperture and the second approximates to a triangular profile with apex angle close to 50°. K_R is calculated from the numerical solution of equation (14) modified as described at the end of section 2·2 by using the degenerate Green's function (17). According to Figure 3(b), Γ_R and Δ_R are periodic functions when $\omega s/U$ exceeds about 2. the particular results shown in Figure 3(c) are typical of all values of $b_1/b_0 < 1$. The real and imaginary parts of K_R again exhibit wavelike variations with frequency, but the waveforms are now sharper than for the square aperture, essentially because singularities (poles) of $K_R(\omega)$ occurring at complex frequencies tend to be closer to the real axis (cf. reference [23]). Equation (2) implies that perturbation energy is dissipated in the aperture when $\Delta_R(\omega) > 0$, and Figure 3 shows that the intervals where this is the case are effectively the same for the square and tapered apertures, except for the first, low frequency interval, where tapering reduces the width of the dissipative zone by about a half. Figure 3(c) also exhibits a gradual decrease with increasing frequency in the amplitude of the oscillations of Γ_R and Δ_R; this is similar to the results given in references [21, 22] for the circular aperture, but does not occur for the square aperture.

3.2. FLOW INSTABILITY FOR FINITE WALL THICKNESS

When the wall has zero thickness ($d = 0$) and the flow is the same on both sides ($U_+ = U_-$), the unsteady aperture motion is stable, in the sense that self-sustaining oscillations cannot be maintained by the extraction of energy from the mean flow. According to equation (2), energy is extracted from the flow at those excitation frequencies in Figure 3 where $\Delta_R(\omega) < 0$. But this instability is *conditional*, inasmuch as the oscillations do not persist once the exciting pressure $[p_0]\,e^{-i\omega t}$ is removed. On the basis of linear theory, absolute instabilities are associated with singularities of the conductivity $K_R(\omega)$ in

$\mathrm{Im}(\omega) > 0$. These singularities are typically simple poles of $K_R(\omega)$; they are eigenvalues of equation (14), and are independent of both $F(\sigma, \xi)$ and the assumption that the driving pressures $p_\pm$ are uniform.

To see this, the integrals over $(-1, +1)$ on the left of equation (14) are discretized by using a convenient Gauss integration formula that expresses them in terms of the integrands evaluated at N lattice points $\xi_i (1 \leqslant i \leqslant N)$. For such a scheme, $\xi_1 = -1 + \delta$, $\xi_N = +1 - \delta$, where $\delta \to +0$ as N becomes large. The Kutta condition (15) is applied by requiring $Z_1 = Z_2 = 0$, where $Z_i \equiv Z(\xi_i)$. The discretized form of equation (14) may then written

$$\sum_{j=1}^{N} \mathfrak{C}_{ij} \bar{Z}_j = F(\sigma, \xi_i), \qquad i = 1 \text{ to } \mathrm{N}, \tag{20}$$

where

$$\bar{Z}_1 = \lambda_+, \bar{Z}_2 = \lambda_- \qquad \text{and} \qquad \bar{Z}_i \equiv Z_i \qquad \text{for} \qquad i \geqslant 3.$$

For each fixed value of i,

$$\mathfrak{C}_{i1} = \mathrm{e}^{\mathrm{i}\sigma_+ \xi_i}, \qquad \mathfrak{C}_{i2} = \mathrm{e}^{\mathrm{i}\sigma_- \xi_i},$$

and $\mathfrak{C}_{ij} (j \geqslant 3)$ depends only on the integration scheme used to approximate the integrals in equation (14). The eigenvalues $\sigma_n = \omega_n s/U$ of equation (20) are the (generally complex) roots of the equation

$$\det(\mathfrak{C}_{ij}) = 0. \tag{21}$$

Cramer's rule [27] and equation (16) now imply that the singularities of $K_R(\omega)$ are poles and coincide with the roots of equation (21). When $U_+ = U_-$ and $d = 0$, they all lie in the lower half of the frequency plane ($\mathrm{Im}\{\omega\} < 0$). The first four ($n = 1$–4, defined such that their positive real parts *increase* with n) have been determined from equation (21) by Newton–Raphson iteration, and are shown by the points labeled "0" in Figure 4 for the case $b_1/b_0 = 0{\cdot}1$ and $b_0/L = 1$. The real parts ω_r of these successive zeros differ by about π, and comparison with Figure 3(c) reveals that they correspond approximately to the real frequencies of the successive minima of $\Gamma_R(\omega)$.

When the wall thickness $d \neq 0$, vortex sheets span the upper and lower faces of the aperture in the absence of external excitation, and the aperture motion must be expected to be unstable. This suggests that the roots of equation (21) cross the real axis into the upper frequency plane, and the curves in Figure 4 show how this occurs for the first four operating stages. Higher order instabilities (n large) are excited first when d/L increases from zero, and all modes are unstable when d/L exceeds about $0{\cdot}02$. When d/L *decreases* from this value, the poles corresponding to $n = 1, 2, 3$, etc., successively cross into the lower half plane; the first four stages are stable when d/L is less than about $7{\cdot}5 \times 10^{-4}$. As d/L increases the complex operating frequencies are seen to converge towards the imaginary axis, their real parts becoming approximately equal; however, the thin wall approximation requires d/L to be small, and probably breaks down before this limiting behaviour is realized. According to the experimental results discussed in reference [16], the real parts of the complex operating frequencies correspond to the Strouhal numbers of self-sustaining oscillations of fluid in the aperture. The dependence of these Strouhal numbers fL/U on d/L (where $f = \mathrm{Re}(\omega)/2\pi$ for a root ω of equation (21)) is illustrated by the solid curves in Figure 5 for the first four operating stages (for $b_0/L = 1$, $b_1/b_0 = 0{\cdot}1$). Each curve starts on the left at that non-zero value of d/L at which the corresponding root of equation (21) crosses into the upper frequency plane. The dotted curves are analogous

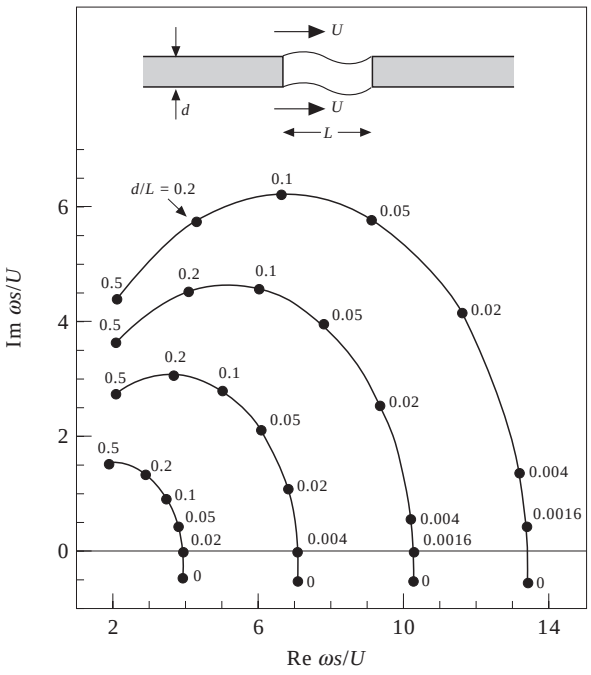

Figure 4. Loci of the complex eigenvalues (zeros of det $(\mathfrak{C}_{ij})$, poles of K_R) for varying d/L, for the first four operating stages when $U_+ = U_- \equiv U$, $b_0/L = 1$, $b_1/b_0 = 0{\cdot}1$.

predictions for the square aperture ($b_0 = b_1$); corresponding modes are seen to become unstable at larger values of d/L. These results imply that the Strouhal numbers of different trapezoidal apertures are approximately the same when based on the *total aperture length* in the streamwise direction.

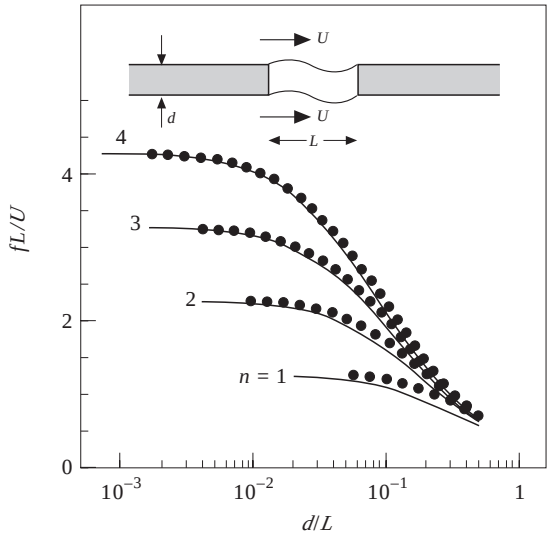

Figure 5. Strouhal number dependence on wall thickness for two-sided uniform flow ($U_+ = U_- \equiv U$) for $b_0/L = 1$: —, $b_1/b_0 = 0{\cdot}1$; ●●●●, $b_1/b_0 = 1$.

It is also instructive to examine the structural changes in $K_R(\omega)$ for real frequencies when d/L increases from zero. The real and imaginary components $\Gamma_R(\omega)$, $\Delta_R(\omega)$ have the near periodic forms shown in Figure 3(c) when $d = 0$ and $b_1/b_0 = 0{\cdot}1$, $b_0/L = 1$. The influence of small, but finite wall thickness is always felt at sufficiently high frequencies, when the second integral on the left of equation (14), which represents the *inertia* of fluid in the aperture, becomes important. This causes the oscillations in the real and imaginary parts of $K_R(\omega)$ ultimately to die out as σ becomes large. The variations of Γ_R and Δ_R for the four different wall thicknesses $d/L = 0{\cdot}007$, $0{\cdot}01$, $0{\cdot}03$ and $0{\cdot}1$ are depicted respectively in Figures 6(a–c). In Figure 6(a) the second stage pole of $K_R(\omega)$ (i.e., the $n = 2$ root of equation (21)) is close to the real axis in the upper frequency plane. When d/L increases to $0{\cdot}01$ the first stage pole is approaching the real axis from below, and this is reflected in Figure 6(b) by the more rapid variations of Γ_R and Δ_R near $\omega R/U = 4$; this pole has crossed the real axis in Figure 6(c), where the former deep minimum of Γ_R is replaced by a sharp maximum, and the variations in Γ_R and Δ_R at higher frequencies are smoother because higher order poles are now further from the real axis. When d/L has increased to $0{\cdot}1$ all of the poles are far from the real axis and the conductivity assumes the characteristic form shown in Figure 6(d), which is very similar to that for *one-sided* flow over the same aperture (see section 4).

4. ONE-SIDED FLOW OVER A TRAPEZOIDAL APERTURE

4.1. THE CONDUCTIVITY FOR ZERO WALL THICKNESS

Let the mean flow be confined to the upper region $x_2 > 1/2d$, over the trapezoidal

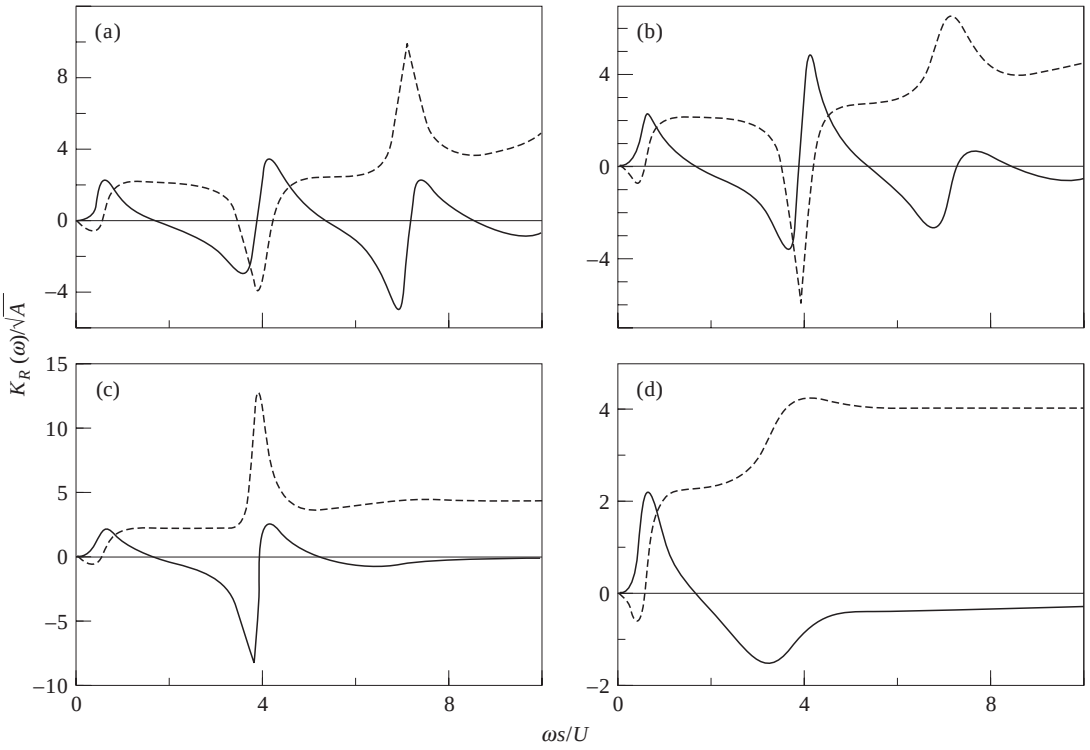

Figure 6. The dependence of $K_R(\omega)/\sqrt{A} = \Gamma_R(\omega) - i\Delta_R(\omega)$ on frequency when $U_- = U_+ \equiv U$, $b_0/L = 1$, $b_1/b_0 = 0{\cdot}1$ and for (a) $d/L = 0{\cdot}007$; (b) $0{\cdot}01$; (c) $0{\cdot}03$; (d) $0{\cdot}1$; —, Δ_R; ---, Γ_R.

aperture of Figure 3(a) (so that $U_- \equiv 0$). In the undisturbed state a vortex sheet separates the uniform flow at speed $U_+ \equiv U$ from the stagnant fluid within and below the aperture. The sheet is unstable for arbitrary wall thickness d, and $K_R(\omega)$ has poles in $\mathrm{Im}(\omega) > 0$. Representative plots of $K_R(\omega)/\sqrt{A}$ for real frequencies are given in Figure 7 for $d = 0$, when $b_0/L = 1$ and $b_1/b_0 = 0{\cdot}01$, $0{\cdot}1$ and 1. All of these plots are structurally similar, and exhibit damping of the applied disturbance by vorticity production when ω is smaller than a critical frequency ω_c, say (where $\Delta_R(\omega) > 0$) which, however, becomes progressively smaller as b_1/b_0 decreases.

They are also similar in form to the conductivity illustrated in Figure 6(d) for two sided, uniform flow ($U_- = U_+$) over a wall of finite thickness $d/L = 0{\cdot}1$, and indeed the conductivity $K_R(\omega)$ for one sided flow over a thin wall also has a similar distribution of instability poles in the upper frequency plane. The variations in the positions of these poles with the ratio b_1/b_0 for the first four stages ($n = 1$–4) are shown in Figure 8 for the case $b_0/L = 1$, $d/L = 0$. By means of the identification $f = \mathrm{Re}(\omega)/2\pi$, the dependence on b_1/b_0 of the corresponding Strouhal numbers fL/U may be calculated; Figure 9 reveals that the Strouhal number changes by about 1/2 between neighboring stages and, in particular (as in the case of two sided flow over a wall of finite thickness, see Figure 5), is only weakly dependent on the shape of the aperture.

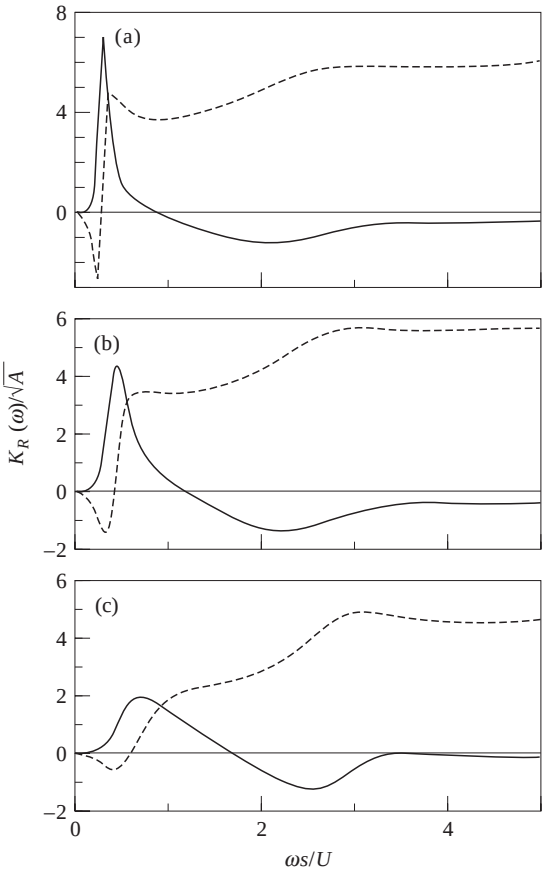

Figure 7. The conductivity $K_R(\omega)/\sqrt{A} \equiv \Gamma_R(\omega) - \mathrm{i}\Delta_R(\omega)$ for one-sided flow ($U_+ \equiv U$, $U_- = 0$) over a trapezoidal aperture when $d/L = 0$, $b_0/L = 1$ and for (a) $b_1/b_0 = 0{\cdot}01$, (b) $0{\cdot}1$ and (c) 1. Key as for Figure 6.

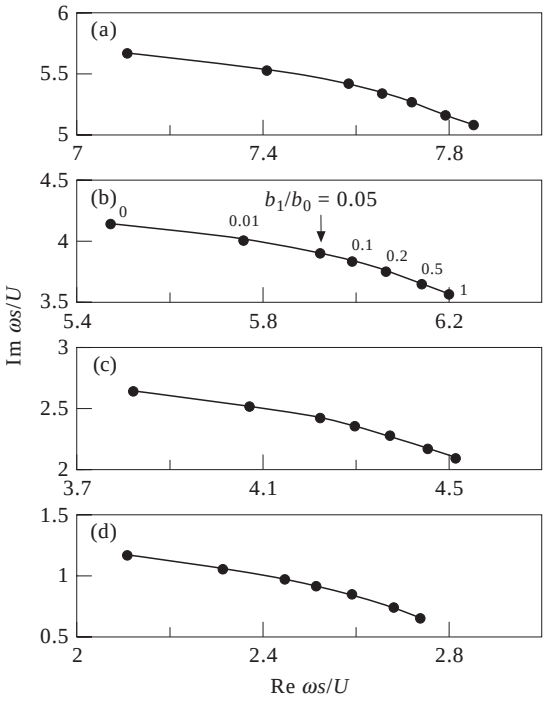

Figure 8. Complex eigenvalues (zeros of $\det(\mathfrak{C}_{ij})$, poles of K_R) for the first four operating stages of one-sided flow ($U_+ = U$, $U_- \equiv 0$) over a trapezoidal aperture when $d/L = 0$ and $b_0/L = 1$, and for $0 < b_1/b_0 < 1$; (a) stage 4, (b) stage 3, (c) stage 2 and (d) stage 1.

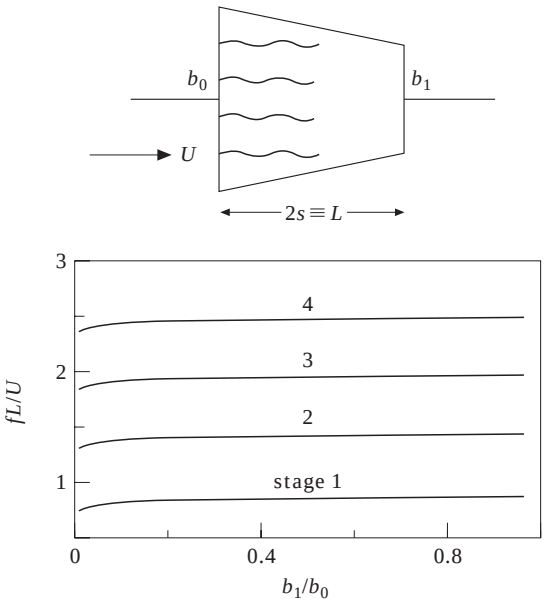

Figure 9. Strouhal number dependence on b_1/b_0 for one-sided flow ($U_+ = U$, $U_- \equiv 0$) over a trapezoidal aperture when $d/L = 0$ and $b_0/L = 1$.

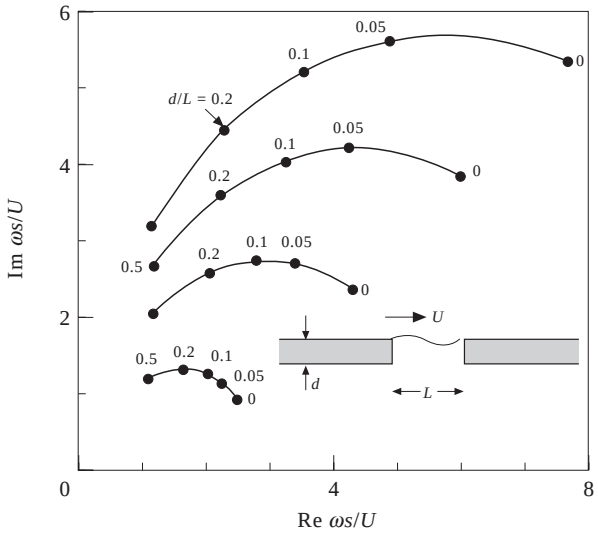

Figure 10. Loci of the complex eigenvalues (zeros of $\det(\mathfrak{C}_{ij})$, poles of K_R) for varying d/L, for the first four operating stages of one sided flow ($U_+ = U$, $U_- = 0$) when $b_0/L = 1$ and $b_1/b_0 = 0{\cdot}1$.

4.2. INFLUENCE OF FINITE WALL THICKNESS

For real values of ω the conductivities $K_R(\omega)$ displayed in Figure 7 do not vary significantly with the trapezoidal shape ratio b_1/b_0. Changes with variations in wall thickness are also small, unlike the case of uniform, two-sided flow discussed in section 3, where $K_R(\omega)$ changes rapidly with d/L because of the passage of poles across the real axis. For one-sided flow, the instability poles are already in $\mathrm{Im}(\omega) > 0$ when $d = 0$, and their subsequent motions in the complex plane when d/L increases from zero produce relatively minor changes in $K_R(\omega)$. The particular case in which $b_0/L = 1$, $b_1/b_0 = 0{\cdot}1$ is illustrated in Figure 10, where the poles of the first four operating stages are tracked (from initial positions given in Figure 8 for $b_1/b_0 = 0{\cdot}1$) in the complex plane as d/L increases over the range 0–0·5. $\mathrm{Re}(\omega s/U)$ is approximately the same for these poles when d/L exceeds about 0·4, implying that Strouhal numbers fL/U of the operating stages become equal, although, as already stressed in section 3, the present thin wall theory may not be strictly applicable for such large values of d/L.

5. CONCLUSION

The properties of unsteady flow induced in a wall aperture by an applied, fluctuating pressure (such as an acoustic disturbance) are significantly affected by the presence of mean flow. At the high Reynolds numbers characteristic of many practical situations, vortex shedding from the aperture edges results in an exchange of energy between the mean flow and the applied pressure. In this paper these interactions have been investigated for a class of apertures whose cross-sections are symmetric with respect to an axis in the mean stream direction and for a wall of small, but finite thickness. Detailed predictions have been given for apertures with tapering (trapezoidal) cross-sections. For two-sided flow, when the mean velocity is the same on both sides of the wall, the motion in the aperture is linearly stable when the wall has zero thickness, but is de-stabilized by finite thickness, when complex eigenfrequencies acquire positive imaginary parts. These eigenfrequencies are poles of the Rayleigh conductivity of the aperture; their values vary in proportion to U/L,

where U is mean flow speed and L is the maximum streamwise length of the aperture, but are only weakly dependent on aperture shape (i.e., on the degree of tapering). A comparison with experiments reported in reference [16] for related physical systems (edge and cavity tones) indicates that the real parts of the complex eigenfrequencies correspond to the tonal frequencies of possible self-sustaining oscillations of the aperture shear layers, the amplitudes of which are controlled by non-linear mechanisms not considered in this paper.

The motion is always unstable for one-sided flow over a wall aperture. In both this case and also for uniform, two-sided flow, increasing the wall thickness causes the eigenfrequencies to progressively decrease, apparently towards a common limiting value for their real parts, although the approximations made in this paper become invalid before this limit is reached. At sufficiently low Strouhal numbers, forced motion of an aperture by an applied pressure is always damped.

ACKNOWLEDGMENTS

This work was sponsored by the Air Force Office of Scientific Research under Grant No. F49620-96-1-0098, administered by Major Brian Sanders.

REFERENCES

1. I. L. Vér 1990 *Noise Control Engineering Journal* **35**, 115–125. Practical examples of noise and vibration control: case history of consulting projects.
2. F. P. Mechel and I. L. Vér 1992 *Sound absorbing materials and sound absorbers*. Chapter 8 of *Noise and Vibration Control Engineering* (eds. L. E. Beranek and I. L. Vér); New York: John Wiley.
3. I. J. Hughes and A. P. Dowling 1990 *Journal of Fluid Mechanics* **218**, 299–336. The absorption of sound by perforated linings.
4. D. Rockwell 1983 *American Institute of Aeronautics and Astronautics Journal* **21**, 645–664. Oscillations of impinging shear layers.
5. J. E. Rossiter 1962 Royal Aircraft Establishment Technical Memorandum 754: *The effect of cavities on the buffeting of aircraft*.
6. F. F. East 1966 *Journal of Sound and Vibration* **3**, 277–287. Aerodynamically induced resonance in rectangular cavities.
7. H. H. Heller and D. B. Bliss 1975 *American Institute of Aeronautics and Astronautics Paper* 75–491. The physical mechanism of flow-induced pressure fluctuations in cavities and concepts for their suppression.
8. N. M. Komerath, K. K. Ahuja and F. W. Chambers 1987 *American Institute of Aeronautics and Astronautics Paper* 87–022. Prediction and measurement of flows over cavities—a survey.
9. K. K. Ahuja and J. Mendoza 1995 *NASA Contractor Report: Final Report Contract* NAS1-19061, *Task* 13. Effects of cavity dimensions, boundary layer, and temperature on cavity noise with emphasis on benchmark data to validate computational aeroacoustic codes.
10. C. K. W. Tam and P. J. W. Block 1978 *Journal of Fluid Mechanics* **89**, 373–399. On the tones and pressure oscillations induced by flow over rectangular cavities.
11. J. C. Bruggeman 1987 *PhD. Thesis*, *Eindhoven University of Technology*. Flow induced pulsations in pipe systems.
12. J. C. Bruggeman, A. Hirschberg, M. E. H. van Dongen, A. P. J. Wijnands and J. Gorter 1989 *Journal of Fluids Engineering* **111**, 484–491. Flow induced pulsations in gas transport systems: analysis of the influence of closed side branches.
13. M. C. A. M. Peters 1993 *PhD Thesis*, *Eindhoven University of Technology*. Aeroacoustic sources in internal flows.
14. J. C. Hardin and D. S. Pope 1995 *American Institute of Aeronautics and Astronautics Journal* **33**, 407–412. Sound generation by flow over a two-dimensional cavity.

15. P. C. Kriesels, M. C. A. M. Peters, A. Hirschberg, A. P. J. Wijnands, A. Iafrati, G. Riccardi, R. Piva and J. C. Bruggeman 1995 *Journal of Sound and Vibration* **184**, 343–368. High amplitude vortex induced pulsations in gas transport systems.
16. M. S. Howe 1997 *Journal of Fluid Mechanics* **330**, 61–84. Edge, cavity and aperture tones at very low Mach numbers.
17. Lord Rayleigh 1945 *Theory of Sound*, Vol 2. New York: Dover.
18. A. Powell 1961 *Journal of the Acoustical Society of America* **33**, 395–409. On the edgetone.
19. D. K. Holger, T. A. Wilson and G. S. Beavers 1977 *Journal of the Acoustical Society of America* **62**, 1116–1128. Fluid mechanics of the edgetone.
20. W. K. Blake and A. Powell 1986 *The development of contemporary views of flow-tone generation*, pp 247–325 *in Recent Advances in Aeroacoustics* (edited by A. Krothapali and C. A. Smith), New York: Springer.
21. M. I. Scott 1995 *Master's thesis*, *Boston University*. *The Rayleigh conductivity of a circular aperture in the presence of a grazing flow*.
22. M. S. Howe, M. I. Scott and S. R. Sipcic 1996 *Proceedings of the Royal Society of London A***452**, 2303–2317. The influence of tangential mean flow on the Rayleigh conductivity of an aperture.
23. M. S. Howe 1996 *Journal of Fluids and Structures* (in press). Influence of wall thickness on Rayleigh conductivity and flow-induced aperture tones.
24. P. Maung, M. S. Howe and S. I. Madanshetty 1996 *Boston University*, *College of Engineering Report No*. AM96–016. Vibration damping of a perforated flap by vorticity production.
25. H. Lamb 1932 *Hydrodynamics* (sixth edition, reprinted 1994) Cambridge University Press.
26. D. G. Crighton 1985 *Annual Reviews of Fluid Mechanics*. **17**, 411–445. The Kutta condition in unsteady flow.
27. G. Dahlquist and Å Björck 1974 *Numerical Methods*. Englewood Cliffs, NJ: Prentice-Hall.
28. M. S. Howe 1975 *Journal of Fluid Mechanics* **67**, 579–610. The generation of sound by aerodynamic sources in an inhomogeneous steady flow.
29. W. Möhring 1979 *Modelling low Mach number noise*, pp 85–96, *Proceedings of the Symposium of Mechanics of Sound Generation in Flows*, Göttingen, August 28–31 (editor E.-A. Müller: Springer, Berlin, 1979).
30. S. M. Grace, K, P. Horan and M. S. Howe 1997 Submitted to *Journal of Fluids and Structures*. The influence of shape on the Rayleigh conductivity of a wall aperture in the presence of grazing flow.